Article

Dynamic Colour Changes in Thermochromic Liquid Crystal Inks: Compatibility with Bacterial Nanocellulose for Sustainable Packaging Solutions

Maja Strižić Jakovljević [1,*], Marta Klanjšek Gunde [2], Tomislav Cigula [1] and Gregor Lavrič [2,3]

[1] Faculty of Graphic Arts, University of Zagreb, Getaldićeva 2, 10000 Zagreb, Croatia; tomislav.cigula@grf.unizg.hr
[2] National Institute of Chemistry, Hajdrihova 19, 1000 Ljubljana, Slovenia; marta.k.gunde@ki.si (M.K.G.); gregor.lavric@icp-lj.si (G.L.)
[3] Pulp and Paper Institute, Bogišićeva 8, 1000 Ljubljana, Slovenia
[*] Correspondence: maja.strizic.jakovljevic@grf.unizg.hr

Abstract: This study investigates the interaction between thermochromic liquid crystal (TLC) inks and bacterial nanocellulose (BNC), emphasizing their compatibility for smart packaging applications. While the chiral nematic structure of TLC pigments dictates their dynamic colour changing behaviour, this research focuses on how TLC inks interact with BNC, a biodegradable and eco-friendly substrate. This study examines material compatibility, colorimetric properties, and the influence of substrate characteristics on the thermally induced colour transitions of TLC inks. Screen printing was employed to deposit TLC inks onto BNC-based films and black uncoated paper, followed by spectrometric analysis to evaluate the temperature-dependent colour response. The results indicate that BNC serves as a promising platform for TLC ink integration, enhancing its potential for intelligent packaging and indicator systems. These findings contribute to the advancement of sustainable, responsive materials for next-generation smart packaging solutions.

Keywords: thermochromic liquid crystals (TLCs); bacterial nanocellulose (BNC); smart packaging; colour play effect; chiral nematic structure

1. Introduction

The chiral nematic (cholesteric) structure of thermochromic liquid crystal (TLC) pigments plays a critical role in the dynamic colour changing properties of TLC printing inks [1,2]. The colour play effect, characterized by transitions from red to blue as temperature increases, is most effective when the inks are applied onto a black substrate [3]. This effect is attributed to the precise structural arrangement of the TLC pigments, which enables their functionality in intelligent applications. Thermochromic inks are widely used in graphic applications, including smart packaging, security printing, brand protection, marketing, and novelty printing, but also in medical applications, toys, and smart textile applications [4–9]. The application of TLC ink to a print is done to produce added value by giving an indication of the product's temperature, security (consumer protection), and/or design and marketing. Some studies also consider the potential applications in nontoxic intelligent sensors, anti-counterfeiting technology, outdoor temperature regulating textiles, wearable temperature sensors, and food packaging industry [10–13].

Thermochromic inks generally consist of microencapsulated thermoresponsive materials in a binder, with the colour change triggered by the activation temperature (T_A) [4,7].

Two primary types of thermoresponsive materials are used: leucodye-based composites (LDs) and thermochromic liquid crystals (TLCs). In both types, the binder plays a critical role in defining the printing and curing processes, while the microencapsulated pigments determine the colour changing behaviour [4,6,8]. In LD types, only two colour states appear, coloured and uncoloured. TLC inks are especially notable for their colour play effect, which occurs within a narrow temperature bandwidth, transitioning from red, orange, yellow, and green to blue as the temperature rises [9]. The colour play effect occurs within the activation region of the TLC ink, where the spectral colour of a given wavelength (λ) becomes visible when the elongated molecules of the active material inside the microcapsules form a helical superstructure with a pitch equal to λ. This material reflects only the light with the corresponding λ (Figure 1) [1,4,6]. In Figure 1, P represents the pitch length of the helix, which is formed by a 360° rotation of the elongated liquid crystal molecules. The pitch length (marked in blue arrow below P in Figure 1) varies with temperature and represents the length at which the vector r in the helix rotates by 360° (vector r represents the orientation of elongated TLC molecules in a monomolecular layer—marked in arrows described by dashed line). The thermochromic effect of TLCs results from this temperature-dependent pitch; as the temperature increases, thermal energy disrupts the liquid crystal alignment, reducing the helical pitch (P). Since the reflected wavelength (λ) is directly proportional to the pitch ($\lambda = n \times P$, where n is the refractive index), a decrease in pitch causes a shift toward shorter (bluer) wavelengths. Consequently, the material's colour transitions from red to blue with increasing temperature [14–17]. The thermochromic effect of TLCs is, therefore, directly related to the structural response of the helical arrangement to temperature variations, with each temperature corresponding to a distinct reflected wavelength and, consequently, a different colour.
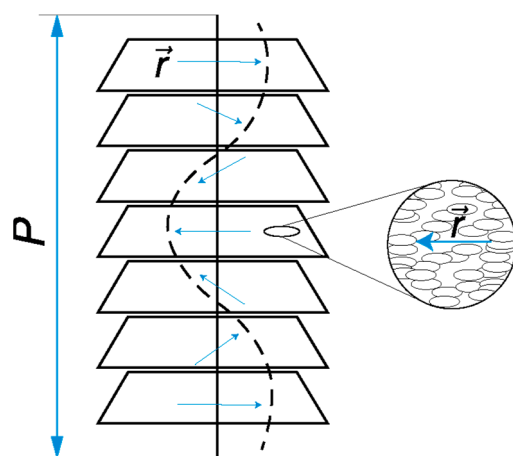

Figure 1. Helical superstructure of the TLCs [2].

Having their working mechanism in mind, thermoresponsive TLC inks offer significant advantages due to their ability to dynamically respond to temperature changes, making them ideal for intelligent packaging solutions. Besides giving added value to packaging solutions, modern packaging must tackle another important challenge—diminishing the packaging's environmental impact. One of the materials with significant potential is cellulose, a natural-based polymer used in various applications. There are many types of cellulose developed, and one of them is bacterial nanocellulose (BNC). Bacterial nanocellulose (BNC) is a type of nanocellulose produced by bacteria and has possible potential for the above purposes. It is a natural, biodegradable, and renewable material that has a variety of potential applications, including as a food additive, a pharmaceutical excipient, a cosmetic ingredient, and a reinforcement agent in composites. Bacterial nanocellulose

can be used in smart packaging applications to improve the performance of packaging materials. It can be used to improve the barrier properties of packaging materials to keep food and other products fresh, and to improve the strength and toughness of packaging materials to prevent them from breaking or tearing. Additionally, bacterial nanocellulose can be used to create packaging materials that are biodegradable and environmentally friendly [10]. Having in mind the positive properties of BNC and thermoresponsive TLC inks, this research focuses on determining the potential application of thermochromic liquid crystal (TLC) inks and bacterial nanocellulose (BNC) as materials for smart packaging. To enable that, an investigation of the TLC and BNC compatibility was conducted, focusing on their material interactions and colorimetric properties.

For this study, BNC-based thin films were prepared, and carbon black was added into their structure to create a suitable printing substrate for TLC inks. The TLC inks were screen printed on black BNC-based films and black uncoated paper, which served as a reference material. Through spectrometric measurements of the printed TLC inks, the influence of the chiral nematic (cholesteric) structure of liquid crystal pigments on the dynamic colour change was examined. The results of the temperature-dependent colour play effect are validated using the communication mechanism developed in our previous research [18]. The distinctive communication mechanism of TLC inks is defined by their temperature-dependent peak in the reflectance spectrum, which serves as a reliable indicator of their structure-induced behaviour. Independent of substrate properties and ink layering, this feature can validate the functionality and compatibility of TLC inks and BNC films [18]. The results of this research could show new possibilities for intelligent and sustainable indicator and packaging solutions. Through combining TLC and BNC, which is a natural, biodegradable, and eco-friendly substrate, the material could gain additional value through its flexibility, UV protection, and printability.

2. Materials and Methods

2.1. Printing Inks and Printing Substrates

In this research, two water-based TLC printing inks for screen printing applications were used. The printing inks are denoted as TLC 14 and TLC 25 (SpotSee, Flintshire, UK) as they differ only in temperature at which the activation region is expected (all other properties are similar). Both TLC 14 and TLC 25 contain microencapsulated TLC pigments dispersed in a water-based binder. The data are given in Table 1, supplied by the manufacturer. TLC 25 becomes red at 25 °C, turns to green at 26 °C, and to blue at 30 °C. Outside the temperature activation region, TLC 25 ink is expected to gradually become colourless, with the complete loss of colour at a clearing point above 44 °C. TLC 14 is activated at 14 °C and develops the entire colour effect within a 5 °C temperature region. The clearing point, where the ink reverts to a colourless state, is reported at about 50 °C. The specifications of the temperature-dependent colour of both inks according to the producer's specifications are presented in Table 1.

Table 1. Temperature-dependent specifications of the used TLC inks.

TLC Ink	TA (°C)	Temperature Activation Region (°C)
TLC 14	14	14–19
TLC 25	25	15–30

TLC inks were screen printed on two types of substrates, black uncoated paper (UT) 200 g/m^2, 630 µm thick, and prepared bacterial nanocellulose (BNC) films, 243 µm thick. Both substrates were black, as TLC requires a minimum optical density (D) of 0.72 for the printing substrates to ensure the colour play effect is clearly visible [3]. Substrate UT is

commercially available in a black colour, while a black colour of the BNC was achieved by adding carbon black to the base material.

2.2. BNC Preparation

Bacterial nanocellulose (BNC) was obtained using a process previously described in our earlier studies, and used for various applications [19–23]. The BNC was sourced as a by-product of the classical static fermentation of apple vinegar. The raw material was extensively washed and purified using a sequential treatment in 50% ethanol at 40 °C, followed by a NaOH solution treatment at the same temperature. The purification steps were performed with constant stirring to remove non-cellulosic impurities. The purified BNC was then homogenized using a high-shear homogenizer. A secondary NaOH treatment was applied to further improve purity.

To prepare the films, 20% (relative to the dry weight of BNC) of PRINTEX 200 carbon black pigment was incorporated into the BNC matrix to create a suitable printing substrate. To improve the dispersion of carbon black and enhance film uniformity, an 8% (relative to the total water content) pigment dispersant (OROTAN™ 165) was added. Before casting the films, black carbon and the dispersant were introduced into the BNC suspension at room temperature under continuous stirring at 600 rpm using a magnetic stirrer. The resulting mixture was then cast onto silicone substrates and dried at 23 °C for 48 h under controlled air circulation.

2.3. Printing Process

Both TLC 14 and TLC 25 were printed in one layer, using a semi-automatic screen printing machine equipped with SEFAR® PET 1500 120/305-40 PW polyester mesh (Sefar AG, Heiden, Switzerland) with a mesh opening of 37 μm [24]. The prints were air-dried before further testing. By activating the dry prints and conducting a visual assessment, the functionality of the temperature-dependent TLC 25 ink was confirmed on both types of substrates before further testing (Figure 2).
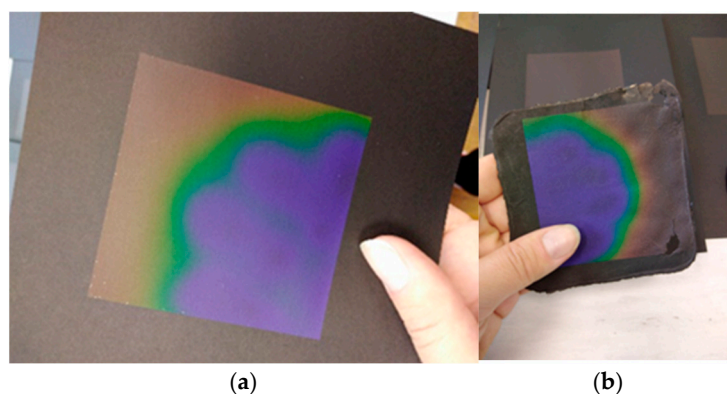

(**a**)   (**b**)

Figure 2. Temperature-dependent optical effect of the TLC 25 ink printed on uncoated black paper (UT) (**a**) and bacterial nanocellulose (BNC) (**b**).

2.4. Characterization of the Printing Substrates

Microscopy was used in order to determine surface morphology, roughness, and average microcapsule size of all samples. For this purpose, a Keyence VHX 7000 digital microscope was used, and the roughness parameters were determined according to ISO 25178:2016 [25]. Thickness of the substrates was measured according to ISO 534:2011 [26]. Measurement of absolute moisture content was performed according to TAPPI–T412 om-94 Moisture in pulp, paper and paperboard, using muffle furnace (Nabertherm L9/11 B180) at 105 °C for 60 min [27]. To determine the content of fillers in

paper substrates and BNC films, the amount of inorganic residue was examined. Ash content was measured at 525 °C and 900 °C, for 60 min, according to the standards TAPPI T 211 om-02 Ash in Wood, Pulp, Paper, and Paperboard: Combustion at 525 °C and TAPPI T 413 om-93 Ash in wood, pulp, paper and paperboard: combustion at 900 °C [28,29].

2.5. Temperature-Dependent Optical Properties of Printed TLC Inks

The optical properties of prints with TLC 14 ink were measured in a temperature range from 9 to 31 °C, and those of prints with TLC 25 were measured between 20 and 38 °C. For this purpose, temperature-dependent spectral reflectance of the samples was measured inside the visible spectral region (400–700 nm) by a fibre-based USB 2000+ spectrometer (Ocean Optics, Orlando, FL, USA) using a 30 mm-wide integrating sphere (ISP-30-6-R) with an (8°: di) measuring geometry and a 6 mm sampling port diameter. OceanView 2.0.18.—EZ software by Ocean Optics was used to calculate the CIELAB L*, a*, b* values, taking into account the D50 illuminant and 2° standard observer. The samples were heated on the surface of a water block (EKWB d.o.o., Ljubljana, Slovenia). In this device, the thermostatically controlled water circulates through very thin acrylic channels inside the base plate. The base plate is made of copper, coated with a nickel layer, and highly polished. Due to very short distances between the water channels and the surface of the plate, the heat from the water is quickly transferred through the plate to the sample. Thus, the temperature of the sample is practically the same as the temperature of the circulating water and measurements can be performed as soon as the temperature of the water in the system reaches the value specified by the thermostat. The applied thermostatic circulator allows a heating rate of about 3.7 °C $\min^{-1}$, and the water temperature is accurate up to a tenth of a degree [9,22].

3. Results

3.1. Surface Morphology

The surface morphology of all samples was determined using a digital microscope with options for 3D surface profiling, measurement, and high-magnification imaging. Three-dimensional imaging and measurement was used for the determination of surface topography and roughness (Figures 3 and 4, Table 2). The roughness values presented in the table were obtained from topographical surface images of all samples. The measurements were recorded to quantify the surface texture characteristics, including average height, peak height, valley depth, and overall height variation. The results provide insight into the effects of using different printing substrates and TLC inks on surface roughness and help in understanding the topographical features of each sample.

Table 2. Roughness parameters for substrates UT and BNC—unprinted and printed with TLC 14 and TLC 25 inks.

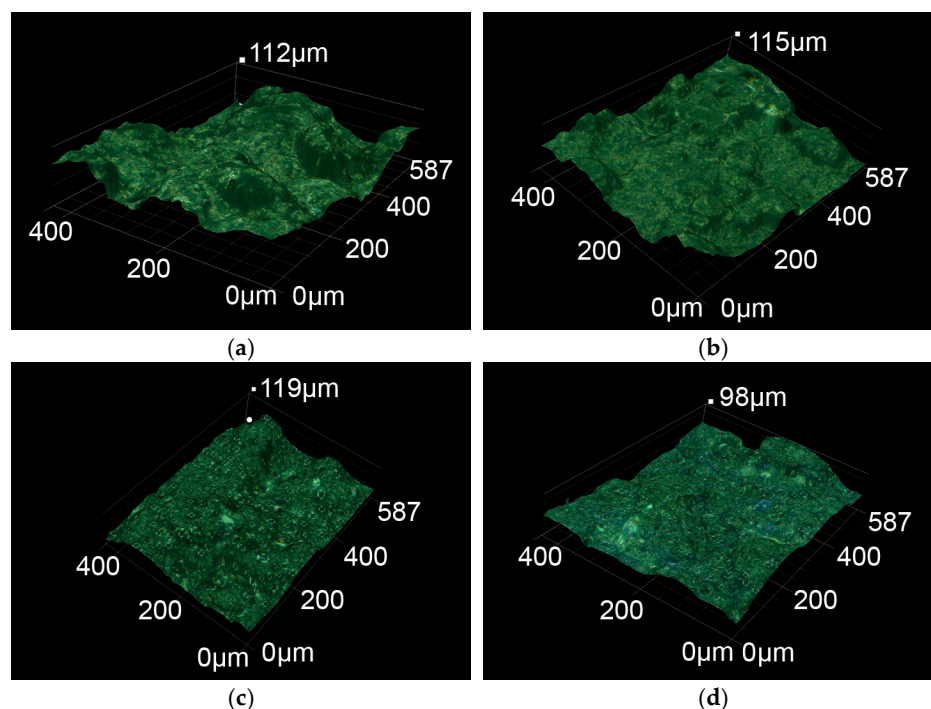| Sample	Sa (µm)	Sz (µm)	Sp (µm)	Sv (µm)
UT, unprinted	2	47	32	15
BNC, unprinted	20	112	47	65
TLC 14 + UT	5	31	15	16
TLC 14 + BNC	18	119	62	57
TLC 25 + UT	3	36	25	11
TLC 25 + BNC	13	97	47	50

Figure 3. Microscopic 3D images of BNC printing substrates: unprinted (**a**,**b**); printed with TLC 14 (**c**); printed with TLC 25 (**d**).
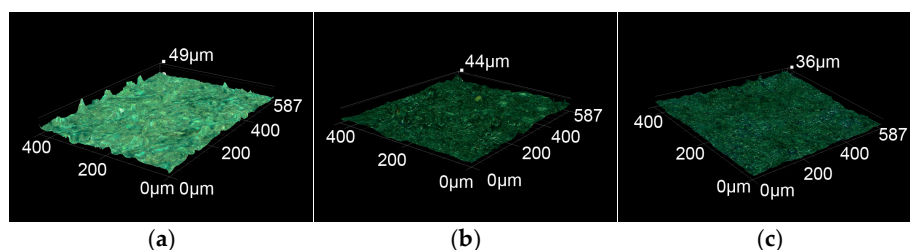

Figure 4. Microscopic 3D images of UT printing substrates: unprinted (**a**); printed with TLC 14 (**b**); printed with TLC 25 (**c**).

The results show the lowest roughness Sa (the average surface height) for UT (2 μm) and a slight increase for TLC 25 + UT (3 μm) (Table 2). TLC 14 + UT displays the smallest height difference Sz (31 μm), which in combination with higher average roughness indicates a more uniform structure with no extreme peaks/valleys on the observed surface (Figure 4c). On the other hand, TLC 25 + UT has a lower average surface roughness than TLC 14 + UT, most probably due to the smaller diameter of the microcapsules (Figure 5). It could be noted that applying ink film onto UT will increase its surface roughness due to the very smooth initial roughness, with microcapsules on the surface increasing roughness. On the other side, BNC has a higher initial surface roughness, and the ink film will fill some valleys and decrease the height of the peaks, i.e., decrease surface roughness. It can also be seen that the BNC sample with TLC 25 has a lower surface roughness, which is probably a consequence of the microcapsules' size.

High-magnification images were also used to determine the pigment morphology and distribution in the printed layer, as well as average size of individual pigment particles (Figure 5).
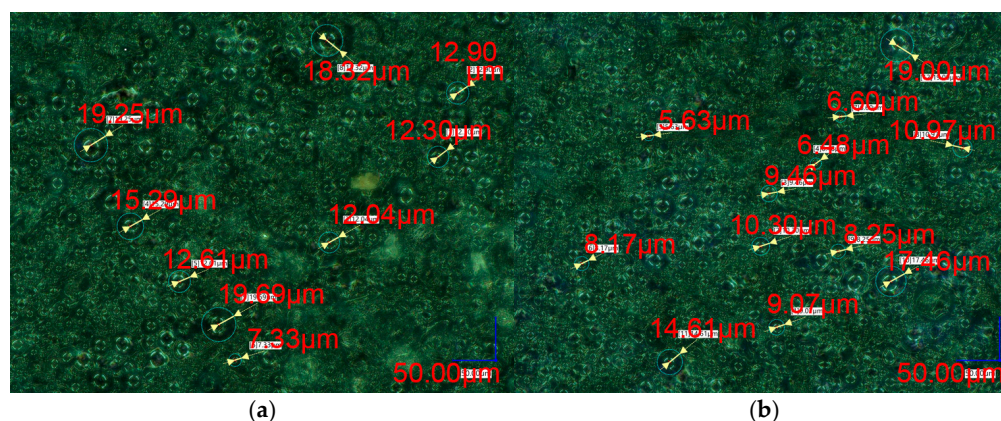
Figure 5. Microscopic 3D images with marked pigment size of printed TLC 14 (**a**); and TLC 25 ink (**b**).

The size of the observed microcapsules of TLC 14 ink (Figure 5a) ranges from 12.04 μm to 19.25 μm, with an average size of 14.41 μm (std. dev. 4.33). The capsules are evenly distributed on the printing samples' surface and exhibit a relatively spherical morphology with no significant agglomeration. The high degree of uniformity in size and shape indicates stable microencapsulation, which is crucial for maintaining the thermochromic performance of the pigment. TLC 25 (Figure 5b) resulted in measured microcapsule sizes from 5.63 μm to 19.07 μm (average of 10.5 μm, std. dev. 4.08), with a broader size distribution compared to TLC 14. This variation could be attributed to differences in the microencapsulation process. Although some smaller particles are visible, the majority maintain a spherical structure. The capsule sizes are within the optimal range for thermochromic applications, ensuring good dispersion in the final product and responsive colour transitions.

3.2. Determination of Fillers Content in UT and BNC Substrates

To determine the ash content, i.e., the amount of fillers in the printing substrates, the absolute moisture content of UT and BNC was measured, and the results are presented in Table 3. The absolute moisture content was later used to calculate the ash content at 525 and 900 °C after the conducted tests. The values of absolute moisture of UT and BNC are nearly identical, indicating that both materials retain a similar amount of moisture before thermal treatment. The combustion experiment was conducted to assess the presence and composition of inorganic fillers in the substrates, which may influence their interaction with TLC inks. The ash residue at 525 °C represents the amount of inorganic components, such as fillers and mineral additives. These inorganic substances can impact the printing process by affecting surface roughness, ink adhesion, and optical properties, which are critical for thermochromic performance. At 525 °C combustion, BNC shows a higher ash content than UT, indicating a higher percentage of inorganic substances, possibly as a residue from the synthesis process of bacterial nanocellulose (e.g., mineral remnants from the nutrient medium). Further combustion at higher temperatures (900 °C) causes degradation of organic substances and potential decomposition of carbonate compounds. The decrease in ash content for BNC from 6.22% to 3.74% suggests the loss of carbonate or other thermally degradable mineral substances. UT also shows a reduction in ash content (from 5% to 4.57%), but to a much lesser extent, which may indicate that paper contains more thermally stable inorganic fillers, such as kaolin or titanium dioxide.

Table 3. The results of moisture and ash content for samples UT and BNC.

Sample	Absolute Moisture (%)	Ash Content/525 °C (%)	Ash Content/900 °C (%)
UT	3.93	5	4.57
BNC	3.93	6.22	3.74

BNC exhibits a greater reduction in ash content from 525 °C to 900 °C, suggesting that its inorganic fraction contains more thermally decomposable or volatile components, likely originating from the bacterial synthesis process (Figure 6a,b). BNC samples after combustion at 525 °C results in a solid black residue, which almost completely disappears at 900 °C, leaving only a few small greenish crystals. The reason for this result could be the addition of an emulsifier to the BNC during sample preparation. In this way, the surface energy of the BNC is changed, which allows greater miscibility with water. The UT substrate retains more stable inorganic content at both temperatures, aligning with its composition of mineral fillers that persist after cellulose combustion (Figure 7a,b).
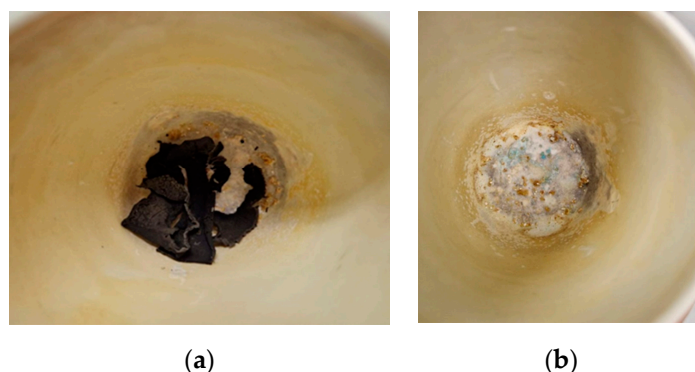

(**a**)　　　　　　　　　　(**b**)

Figure 6. Samples of BNC substrate after the combustion at 525 °C (**a**), and 900 °C (**b**).

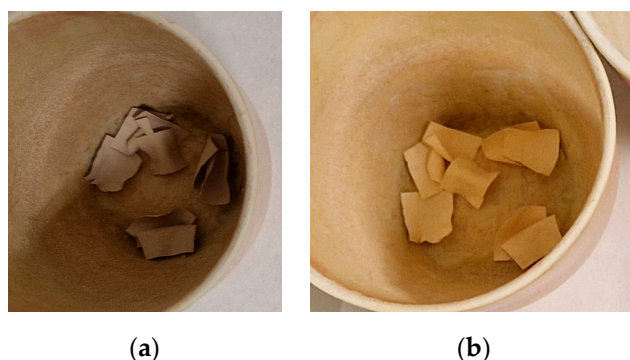(**a**)　　　　　　　　　　(**b**)

Figure 7. Samples of UT substrate after the combustion at 525 °C (**a**), and 900 °C (**b**).

3.3. Temperature-Dependent Colorimetric Properties of Printed TLC Inks

The results presented in Figures 8–11 show the temperature-dependent colorimetric response of printed TLC inks. As mentioned above, with the increase in temperature, the helical pitch of thermochromic liquid crystals (TLCs) shrinks and results in the reflection of light with progressively shorter wavelengths. This structural transformation shows as a spectral colour change from red (longer wavelengths) to blue (shorter wavelengths). The thermochromic effect is directly linked to the ratio between the helical spiral length and pitch, with each temperature corresponding to a specific reflected wavelength and, consequently, a distinct observed colour. The spectral characteristic of the colour play effect is a relatively narrow single reflection peak that occurs when the functional material inside the pigments is in the chiral nematic/cholesteric phase. This peak moves across the visible range as a function of the temperature and is confirmed for both TLC inks and substates in this research (Figures 8–11).
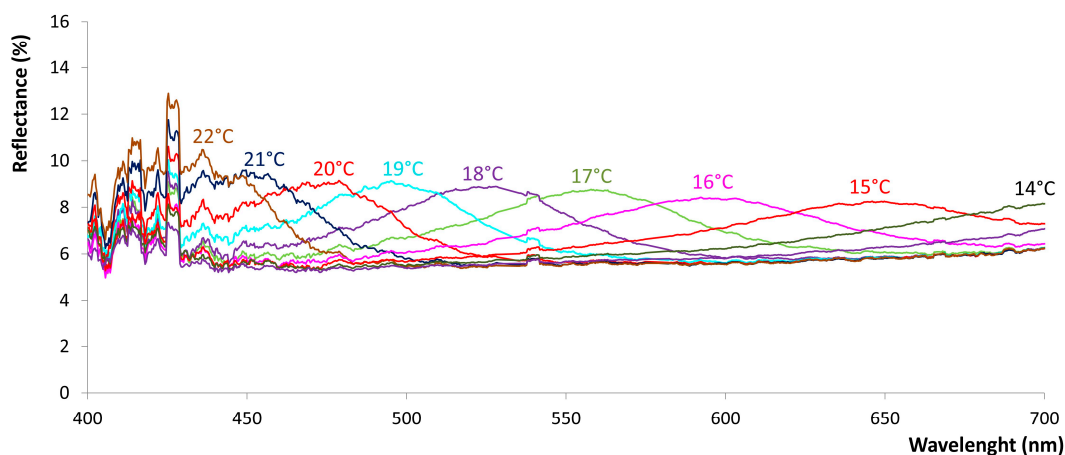
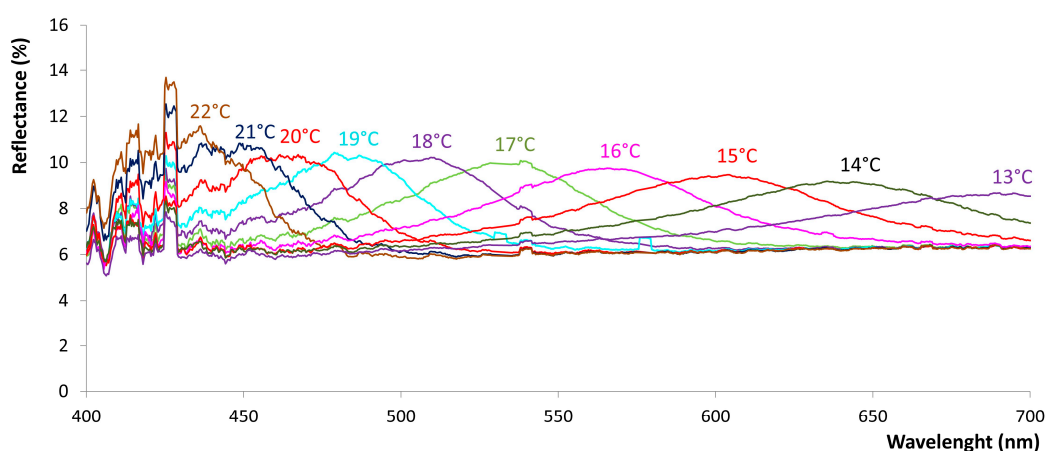**Figure 8.** Reflectance spectra of TLC 14 ink printed on UT substrate.

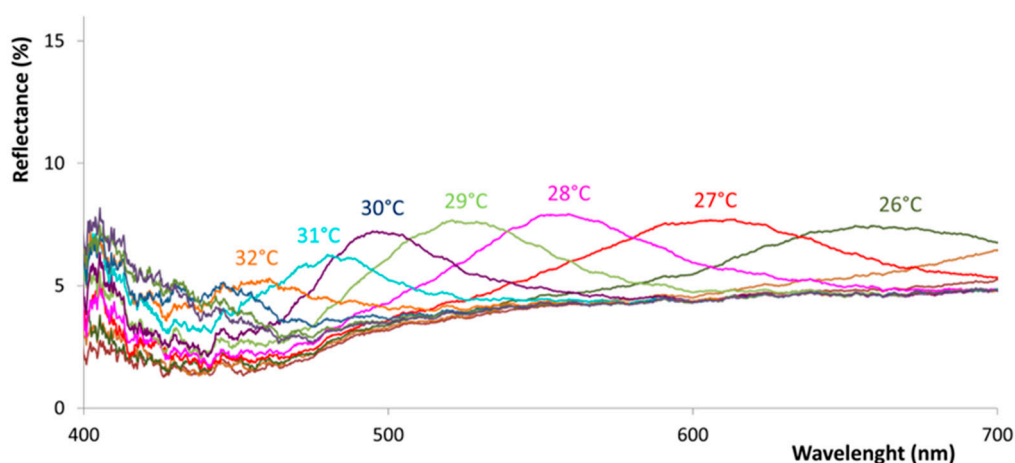**Figure 9.** Reflectance spectra of TLC 14 ink printed on BNC substrate.

Figure 10. Reflectance spectra of TLC 25 ink printed on UT substrate.

For TLC 14 ink printed on a UT substrate, the chiral nematic phase of the liquid crystalline material is formed at 14 °C, where a low and broad reflectance peak appears at the long wavelength limit of the visible (700 nm) (Figure 8). At 15 °C, this peak shifts to 646 nm and the sample appears orange/red. A further increase in temperature shifts the peak throughout the visible spectrum to shorter wavelengths, making it slightly narrower and a bit more intense. These changes are not linearly dependent on the temperature, so that the blue part of the spectrum remains visible most of the time. This corresponds to

the visual perception of the sample—its appearance is very distinctly blue and remains as such over the widest temperature range. As the temperature rises above 22 °C, the peak becomes hardly visible. A further increase in temperature shifts the peaks outside of the visible region and they disappear completely above the clearing point of 50 °C, because the TLC turns into an isotropic liquid. Similar results are noticed for TLC 14 printed on BNC, apart from the formation of a chiral nematic phase occurring at 13 °C and 692 nm (Figure 9). This shift is most likely caused by the selection of printing substrate.
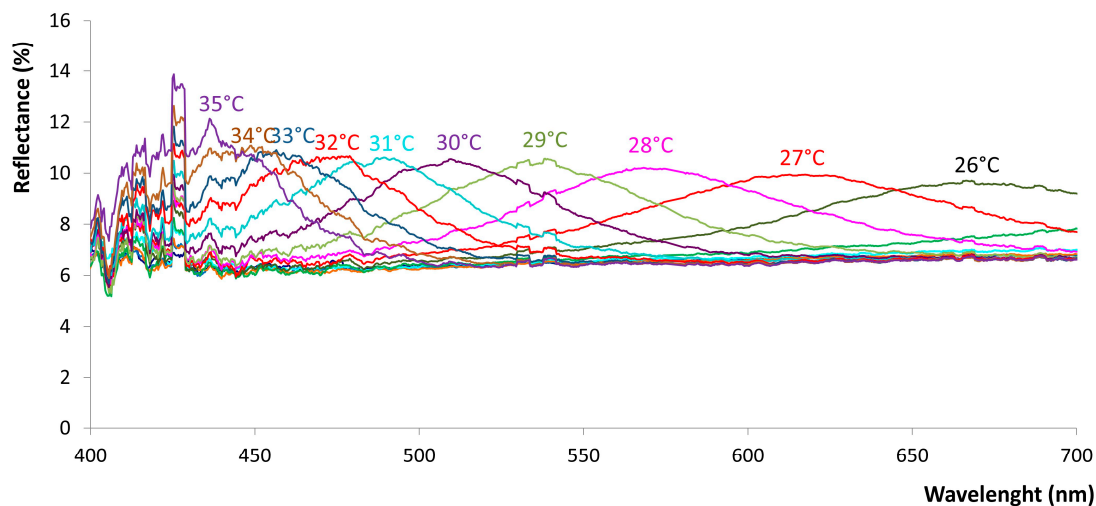

Figure 11. Reflectance spectra of TLC 25 ink printed on BNC substrate.

For TLC 25 ink printed on a UT substrate, the chiral nematic phase of the liquid crystalline material is formed at 26 °C and 665 nm (Figure 10). A further increase in temperature shifts the peak throughout the visible spectrum to shorter wavelengths, showing the full colour play effect. Similarly to TLC 14, the peak becomes hardly visible at higher temperatures, in this case above 32 °C. A further increase in temperature gradually leads to turning TLC into an isotropic liquid and the loss of colour play effect. The reflection maximum is similar for TLC 14 on UT and BNC substrates, while for TLC 25 they differ and have higher values for the prints on BNC where the baseline is higher and more stable compared to TLC 25 on a UT substrate (Figure 11). Additionally, the maximum of reflection spectra can be observed up to 35 °C for TLC 25 on BNC, whereas on UT it can only be observed until 32 °C. Both TLC 14 and TLC 25 exhibited a broader activation range than that defined by the specifications (Table 1).

The chromaticity of the colour play effect is described using the a* (green–red) and b* (blue–yellow) CIELAB coordinates, derived from the corresponding reflectance spectra measured on the same samples (Figures 8–11). Each point on the curve represents the chromaticity of the sample at a specific temperature (Figure 12). As the temperature increases (in the steps of 1 °C), the points move anticlockwise across the four quadrants of the (a*, b*) plane (blue arrows in Figure 12). This movement forms a closed loop, characteristic of the colour play effect observed in activation region of the TLCs. The red–green (a*) and yellow–blue (b*) values begin and end at nearly identical positions on the (a*, b*) graph for all samples, representing the isotropic phase of the TLC, where no colour is developed, i.e., at the point of printing substrate colour. At intermediate temperatures, where the chiral-nematic (cholesteric) phase generates a single reflection peak (Figures 8–11), the complete loop is formed, illustrating the thermochromic effect. A similar curve shape across all samples demonstrates that each printed sample undergoes a colour change across the entire visible spectrum. Moreover, the results confirm that incorporating BNC does not diminish the optical properties of the TLC and enables the

dynamic colour change caused by chiral-nematic (cholesteric) phase. Among the tested samples, however, TLC 14 + UT stands out by exhibiting the narrowest curve, particularly in the yellow–green region of the diagram, while the remaining samples show only minor differences from one another. The differences in the presented results are very small, confirming the visual appearance of the prints within the activation region of the inks (Figure 12).
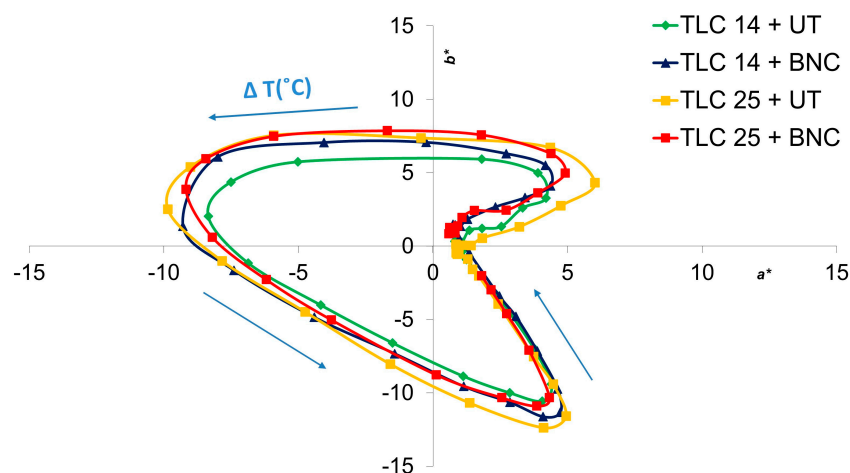

Figure 12. CIELAB colour values of the TLC 14 and TLC 25 ink printed on UT and BNC substrates, measured by spectrometer and presented in (a*, b*) diagram.

In addition to the CIELAB chromatic values a* and b*, the colour values also include L* (lightness), as shown in Figure 13. Both TLC 14 + UT and TLC 14 + BNC span a temperature range from 9 to 31 °C, while for TLC 25 + UT and TLC 25 + BNC the range extends from 20 to 38 °C. The activation region of both inks occurs inside this ranges and corresponds with the reflection peaks in the visible spectrum (Figures 8–11). Each L*(T) curve exhibits a single maximum in the green region, where the colour reaches its highest lightness (L*max) value (Table 4). The results indicate an increase in L* values within the activation range of the TLC ink, which, according to the manufacturer's specifications (Table 1), is between 14 and 19 °C for TLC 14 and between 15 and 30 °C for TLC 25. However, the results in Figure 13 reveal a shift in the activation range for the printed TLC inks to approximately 9–23 °C for TLC 14 and 21–35 °C for TLC 25. For the samples printed on BNC, L* has higher values compared to the samples printed on UT substrates. However, these differences are not significant, as the L* value for TLC 14 is 1.28 and for TLC 25 is 0.65 in favour of BNC. This result is most likely influenced by the colorimetric properties of the substrates themselves.

Table 4. Properties of TLC inks printed on a UT and BNC substrate: temperature at which the L*(T) curve has its maximum is denoted by T(L*max), and its intensity by ΔL*max. See also Figure 13.

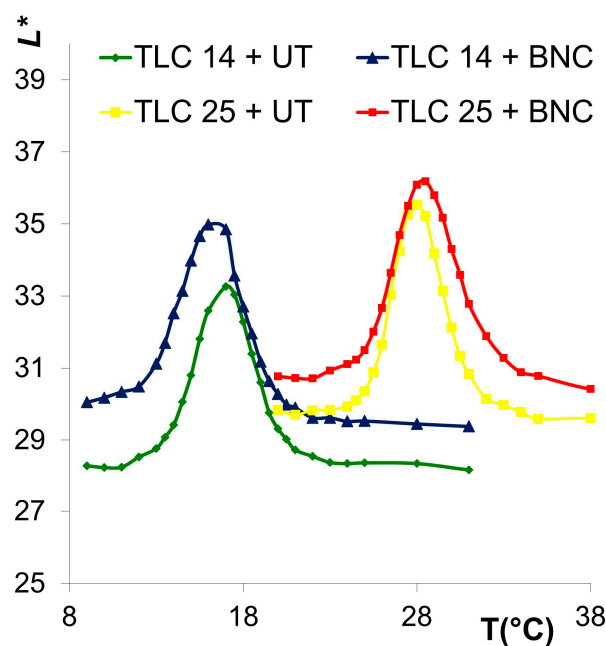| TLC Prints	T(L*max) (°C)	λ (nm)	ΔL*max
TLC 14 + UT	17	556	5.09
TLC 14 + BNC	16	566	5.6
TLC 25 + UT	28	555	5.94
TLC 25 + BNC	28.5	554	5.76

Figure 13. Temperature dependence of CIELAB lightness values L*, measured for TLC 14 and TLC 25 printed on UT and BNC substrates.

It is important to emphasize that all selected combinations of TLC inks and substrates enable a full thermochromic effect, which is manifested through the colour play effect, characteristic reflectance spectra and CIELAB L*a*b* chromatic values (Figures 8–12). These results describe the influence of the chiral nematic (cholesteric) structure of liquid crystal pigments on the dynamic colour change.

The so-called communication mechanism, the method used for describing temperature-dependent colour play effect of the TLCs, is introduced in one of our previous research projects and is applied here to verify structurally induced behaviour of TLC pigments [11]. The temperature-sensitive peak in the reflectance spectra can serve as a reliable indicator of TLC functionality and compatibility with selected substrates. The communication mechanism of all samples shown in Figure 14 demonstrates the temperature dependence of the peak in the reflectance spectra. As the temperature increases, these peaks shift to shorter wavelengths, which is the effect characteristic for TLC inks (commonly called colour play effect). To the best of our knowledge, TLC inks are the only type of printing inks that can be described using the proposed communication mechanism. The results in Figure 14 are presented in two diagrams due to different temperature ranges of TLC 14 and TLC 25, corresponding to the activation regions of the ink. These results are based on the extracted wavelengths at which the reflectance peaks appear—λmax—and presented as variables of the temperature. The results show curves with similar trends, deviating for each TLC colour due to differences in the reflection spectra measured on UT and BNC substrates. It can be seen that the communication mechanism is almost the same for TLC25 ink on both substrates, but for TLC14, some differences appear at low temperatures. Despite these minor differences, the communication mechanism confirms the functionality of TLC inks through authentic characterization within the activation range. These results confirm the compatibility of TLC inks with the BNC substrate, which could contribute to the development of new intelligent and sustainable solutions in the future.
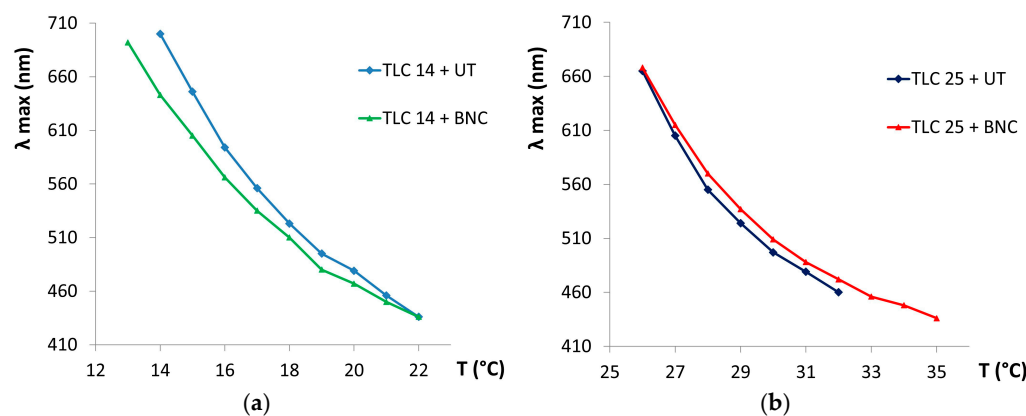
Figure 14. Position of the reflectance peak dependent on temperature for TLC 14 (**a**), and TLC 25 ink (**b**), printed on UT and BNC substrates (referring to Figures 8–11).

4. Conclusions

In this study, BNC based, thin films were prepared, with carbon black added to create a suitable printing substrate for TLC inks. The TLC inks were screen printed onto BNC as well as black uncoated paper (UT), which was used as a reference. Microscopic images were taken and analyzed to enable determination of the printed surface and microcapsules spread. Spectrometric measurements of the printed TLC 14 and TLC 25 inks were conducted to investigate the impact of the chiral nematic (cholesteric) structure of liquid crystal pigments on dynamic colour change.

The results of the measured roughness parameters showed significant difference between the two substrates, with BNC having higher roughness. These are transferred to the roughness of the printed samples, i.e., prints on the BNC show higher roughness than the ones on UT. Furthermore, prints made by applying TLC 14 have higher average roughness than those which had TLC 25 applied.

Spectrometric measurements showed the observed colour transitions which confirm the structural behaviour of TLCs and demonstrate their precise and repeatable colour changes across a defined temperature range. This effect occurs for both TLC 14 and TLC 25 printed either on UT or on BNC. The results of the CIELAB colour measurements indicate that the BNC exhibits slightly higher lightness (L) values compared to UT, suggesting that surface roughness may influence the way light interacts with the printed layers. Given that rougher surfaces can alter light scattering and absorption, the increased roughness of BNC + TLC materials may enhance the optical response by modifying reflectance, potentially improving colour visibility for consumer applications.

The results of the temperature-dependent colour play effect are validated using the communication mechanism developed in our previous research. This distinctive feature of TLC inks is defined by their temperature-dependent peak in the reflectance spectrum, which serves as a reliable indicator of their structure-induced behaviour. The results validate the functionality and compatibility of TLC inks and BNC. It is essential to highlight that all selected combinations of TLC inks and substrates achieve a complete thermochromic effect, characterized by the colour play effect, shown in the results of reflectance spectra and CIELAB L*a*b* chromatic values. These results describe the impact of the chiral nematic (cholesteric) structure of liquid crystal pigments on dynamic colour change. The results of CIELAB a*b* chromatic values describing the colour play effect show the differences between all samples, but are not significant, while the results of CIELAB lightness values L* show that BNC exhibits slightly higher values compared to UT. These results are most likely influenced by the properties of the selected substrates.

Although the communication mechanism confirms the functionality and compatibility of the selected TLC inks and BNC, certain deviations occur when compared to the results measured on the UT. These differences are more pronounced in TLC 14 than in TLC 25, particularly at lower temperatures. Further research is needed to determine the factors influencing these minor discrepancies. Possible reasons for these variations may be related to specific characteristics of the printing substrates, such as surface roughness, as well as the distribution and size of the microcapsules on the dried TLC layer.

To conclude, bacterial nanocellulose was proven to be a functional and compatible material for TLC inks and could present a promising solution for sustainable and dynamic packaging/indicator applications in the future. The surface properties of BNC appear to influence the optical response of TLC inks, which could be leveraged to optimize thermochromic visibility for consumer-facing applications. The advantages of the BNC material properties as a printing substrate, such as flexibility, UV protection, printability, and biodegradability, could offer added value to the packaging solutions and their interaction with TLCs should be studied in detail in the future.

References

1. Taugerbeck, A.; Booth, C.J. Design and Synthesis of Chiral Nematic Liquid Crystals. In *Handbook of Liquid Crystals*; Wiley: Hoboken, NJ, USA, 2014; pp. 1–63. [CrossRef]
2. LCR Hallcrest. Hallcrest Handbook of Thermochromic Liquid Crystal Technology.pdf. Available online: https://spotsee.io/wp-content/uploads/2021/05/RT006-Rev01-USA-Thermochromic-Handbook.pdf?srsltid=AfmBOoqBS9yrfgobRIj48S7Q0KwbZ3_zI2FCF3ukTqJNEUCaJuqjSR95 (accessed on 1 October 2024).
3. Strižić Jakovljević, M.; Lozo, B.; Klanjšek Gunde, M. The properties of printing substrates required for thermochromic liquid-crystal printing inks. *J. Print Media Technol. Res.* **2018**, *7*, 165–170. [CrossRef]
4. Seeboth, A.; Lötzsch, D.; Ruhmann, R.; Muehling, O. Thermochromic polymers—Function by design. *Chem. Rev.* **2014**, *114*, 3037–3068. [CrossRef] [PubMed]
5. Christie, R.M.; Robertson, S.; Taylor, S. Design Concepts for a Temperature-sensitive Environment Using Thermochromic Colour Change. *Colour Des. Creat.* **2007**, *1*, 1–11.
6. White, M.A.; LeBlanc, M. Thermochromism in Commercial Products. *J. Chem. Educ.* **1999**, *76*, 1201–1205. [CrossRef]
7. Kerry, J.; Butler, P. *Smart Packaging Technologies for Fast Moving Consumer Goods*; Wiley: Hoboken, NJ, USA, 2008. [CrossRef]
8. Zhang, W.; Fei, L.; Zhang, J.; Chen, K.; Yin, Y.; Wang, C. Durable and tunable temperature responsive silk fabricated with reactive thermochromic pigments. *Prog. Org. Coat.* **2020**, *147*, 105697. [CrossRef]
9. Štaffová, M.; Kučera, F.; Tocháček, J.; Dzik, P.; Ondreáš, F.; Jančář, J. Insight into color change of reversible thermochromic systems and their incorporation into textile coating. *J. Appl. Polym. Sci.* **2021**, *138*, 49724. [CrossRef]
10. Liu, B.; Rasines Mazo, A.; Gurr, P.A.; Qiao, G.G. Reversible Nontoxic Thermochromic Microcapsules. *ACS Appl. Mater. Interfaces* **2020**, *12*, 9782–9789. [CrossRef] [PubMed]
11. Geng, X.; He, Y.; Han, N.; Zhang, X.; Li, W. Synthesis and characterization of hydrophobic reversible thermochromic MicroPCMs with amino resins shell for thermal energy storage. *Energy Build.* **2021**, *230*, 110528. [CrossRef]
12. He, Y.; Li, W.; Han, N.; Wang, J.; Zhang, X. Facile flexible reversible thermochromic membranes based on micro/nanoencapsulated phase change materials for wearable temperature sensor. *Appl. Energy* **2019**, *247*, 615–629. [CrossRef]
13. Breheny, C.; Donlon, K.; Harrington, A.; Colbert, D.M.; Bezerra, G.S.N.; Geever, L.M. Thermochromic Polymers in Food Packaging: A Comprehensive Systematic Review and Patent Landscape Analysis. *Coatings* **2024**, *14*, 1252. [CrossRef]

14. Sage, I. Thermochromic liquid crystals. *Liq. Cryst.* **2011**, *38*, 1551–1561. [CrossRef]

15. Lagerwall, J.P.F.; Scalia, G. A new era for liquid crystal research: Applications of liquid crystals in soft matter nano-, bio- and microtechnology. *Curr. Appl. Phys.* **2012**, *12*, 1387–1412. [CrossRef]

16. Kitzerow, H.-S.; Bahr, C. *Chirality in Liquid Crystals*; Springer: New York, NY, USA, 2001.

17. Yoon, J.; Lee, W.; Thomas, E.L. Thermochromic block copolymer photonic gel. *Macromolecules* **2008**, *41*, 4582–4584. [CrossRef]

18. Jakovljević, M.S.; Lozo, B.; Gunde, M.K. Identifying a unique communication mechanism of thermochromic liquid crystal printing ink. *Crystals* **2021**, *11*, 876. [CrossRef]

19. Dermol, Š.; Borin, B.; Gregor-Svetec, D.; Slemenik Perše, L.; Lavrič, G. The Development of a Bacterial Nanocellulose/Cationic Starch Hydrogel for the Production of Sustainable 3D-Printed Packaging Foils. *Polymers* **2024**, *16*, 1527. [CrossRef] [PubMed]

20. Lavrič, G.; Medvešček, D.; Skočaj, M. Papermaking properties of bacterial nanocellulose produced from mother of vinegar, a waste product after classical vinegar production. *Tappi J.* **2020**, *19*, 197–203. [CrossRef]

21. Lavrič, G.; Oberlintner, A.; Filipova, I.; Novak, U.; Likozar, B.; Vrabič-Brodnjak, U. Functional Nanocellulose, Alginate and Chitosan Nanocomposites Designed as Active Film Packaging Materials. *Polymers* **2021**, *13*, 2523. [CrossRef] [PubMed]

22. Mahović Poljaček, S.; Tomašegović, T.; Strižić Jakovljević, M.; Jamnicki Hanzer, S.; Murković Steinberg, I.; Žuvić, I.; Leskovac, M.; Lavrič, G.; Kavčič, U.; Karlovits, I. Starch-Based Functional Films Enhanced with Bacterial Nanocellulose for Smart Packaging: Physicochemical Properties, pH Sensitivity and Colorimetric Response. *Polymers* **2024**, *16*, 2259. [CrossRef] [PubMed]

23. Pantić, M.; Nowak, M.; Lavrič, G.; Knez, Ž.; Novak, Z.; Zizovic, I. Enhancing the properties and morphology of starch aerogels with nanocellulose. *Food Hydrocoll.* **2024**, *156*, 110345. [CrossRef]

24. Sefar AG. SEFAR® PET 1500. Available online: https://www.sefar.com/data/docs/zh/10855/PS-PDF-SEFAR-PET1500-AL-EN.pdf?v=1.8 (accessed on 11 December 2024.).

25. *ISO 25178:2016*; Geometrical Product Specifications (GPS)—Surface Texture: Areal. ISO: Geneva, Switzerland, 2016.

26. *ISO 534:2011*; Paper and Board—Determination of Thickness, Density and Specific Volume. ISO: Geneva, Switzerland, 2011.

27. *TAPPI-T412*; Om-94 Moisture in Pulp, Paper and Paperboard. TAPPI: Peachtree Corners, GA, USA, 2016.

28. *TAPPI T 211*; Om-02 Ash in Wood, Pulp, Paper, and Paperboard: Combustion at 525 °C. TAPPI: Peachtree Corners, GA, USA, 2007.

29. *TAPPI T 413 93*; Ash in Wood, Pulp, Paper and Paperboard: Combustion at 900 °C. TAPPI: Peachtree Corners, GA, USA, 2007.